O 1s near-edge x-ray absorption of La2-xSrxNiO4+delta: Holes, polarons, and excitons

Pellegrin, E.; Zaanen, J.; Lin, H.J.; Meigs, G.; Chen, C.T.; Ho, G.H.; ... ; Uchida, S.

O 1*s* near-edge x-ray absorption of $La_{2-x}Sr_xNiO_{4+\delta}$: Holes, polarons, and excitons

E. Pellegrin*
AT&T Bell Laboratories, 600 Mountain Avenue, Murray Hill, New Jersey 07974

J. Zaanen
Lorentz Institute for Theoretical Physics, Leiden University, P.O. Box 9506, NL-2300 RA Leiden, The Netherlands

H.-J. Lin,† G. Meigs, and C. T. Chen†
AT&T Bell Laboratories, 600 Mountain Avenue, Murray Hill, New Jersey 07974

G. H. Ho†
Department of Physics, University of Pennsylvania, Philadelphia, Pennsylvania 19104

H. Eisaki and S. Uchida
Superconductivity Research Course, The University of Tokyo, Bunkyo-Ku, Tokyo 113, Japan
(Received 2 May 1995)

Polarization-dependent near-edge x-ray absorption spectroscopy measurements have been performed on the O 1*s* and Ni 2*p* edges of $La_{2-x}Sr_xNiO_{4+\delta}$ single crystals for $0 \leqslant x \leqslant 0.6$. The results are compared with recent data on $La_{2-x}Sr_xCuO_{4+\delta}$, and NiO and with detailed cluster calculations on a NiO_6 cluster. From this, we determine the energetic ordering of the states close to the Fermi level with Ni(Cu) $3d_{x^2-y^2}$/O $2p_{x,y}$ and Ni(Cu) $3d_{3z^2-r^2}$/apex-O $2p_z$ orbital character for the undoped compounds. We find that *d-d* exciton side bands show up in the final states of $La_{2-x}Sr_xNiO_{4+\delta}$, giving evidence for the Zhang-Rice character of the doped carriers. The spectral-weight transfer in the O 1*s* spectra shows a significant dynamical component. Thus, we suggest that the polarons in $La_{2-x}Sr_xNiO_{4+\delta}$ can be seen as nonclassical objects on the length scale of a lattice constant and that the formation of polaron domain walls and polaron lattices possibly has to be considered as a result of this large coherence length of the polarons.

I. INTRODUCTION

The electronic structure of $La_{2-x}Sr_xNiO_{4+\delta}$ (LSNO) has been a controversial issue for a long time because of its interesting magnetic, transport, and structural properties.[1,2] Although it is closely related to the isostructural high-temperature superconductor $La_{2-x}Sr_xCuO_{4+\delta}$ (LSCO), the transport properties of these two materials are quite different. It seems now to be established that the nickelate does not become superconducting even at very low temperatures. This is in contrast to earlier studies reporting the occurrence of superconductivity in this system.[3]

It is now becoming increasingly clear that the nickelates are interesting systems on their own, which show rich physics and complex phenomena such as electron correlation and polaron localization. There is now both experimental and theoretical evidence for the electron-phonon coupling as the main reason for the insulating behavior of the doped nickelates. On the experimental side, Strangfeld *et al.*[4] pointed out the polaronic character of the doped charge carriers in LSNO. An estimate for the polaron localization energy of ~ 0.2 eV has been given by Bi and Eklund[5] from optical conductivity data. This is in agreement with calculations by Anisimov *et al.*,[6] which also stress the importance of stronger self-localization effects for holes in LSNO as compared to LSCO. They conclude that the reason for this is the interplay of a planar breathing-type lattice relaxation of the NiO_6 octahedron and an enhanced magnetic confinement in the nickelate leading to the formation of small polarons in LSNO. A detailed theoretical analysis of the mechanisms leading to the formation of polaron lattices and domain walls in LSNO has been performed by Zaanen and Littlewood.[7] According to their results this is made possible due to the positive feedback between the the electron-phonon coupling and the ordering tendencies given by the Zhang-Rice[8] localization.

In a recent electron diffraction study, Chen *et al.*[9] demonstrated charge ordering in the form of a polaron lattice at higher doping concentrations in $La_{1.5}Sr_{0.5}NiO_{4+\delta}$. For the lower-doping regime ($La_2NiO_{4.125}$) Tranquada *et al.*[10] showed by means of single-crystal neutron diffraction that at lower doping the holes order in domain walls that form antiphase boundaries between antiferromagnetic domains in the ordered Néel background and which line up to form a striped phase.

Up to now, near-edge x-ray absorption spectroscopy (NEXAFS) has provided a significant contribution to the understanding of the underlying physics in the undoped and doped transition metal oxides. The issue of whether Li-doped NiO also has to be considered as a charge-transfer insulators or as being in the intermediate regime between Mott-Hubbard and charge-transfer insulators[11] is still under debate. Direct evidence for the charge-transfer nature of LSCO has come from electron energy-loss spectroscopy[12] (EELS) and NEXAFS.[13,14] This was accomplished by showing that the intrinsic hole has predominantly Cu $3d_{x^2-y^2}$ character with a small admixture of O $2p_{x,y}$ states, whereas the doped

holes have predominantly planar O $2p_{x,y}$ character with a small admixture of Cu $3d_{x^2-y^2}$ orbitals. The so-called spectral-weight transfer effect, occurring as a function of doping and directly seen in NEXAFS, was used to make a strong case for the effective single-band Mott-Hubbard nature of the carrier states.[15]

The spectral-weight transfer effects, i.e., the redistribution of weight between high- and low-energy bands due to changes in the hole concentration, have been extensively investigated especially in the cuprate superconductors. The effect is theoretically well understood, at least to the extent that it is clear which microscopic quantities are actually measured.[16,15,17–19] At the same time, one can question the significance of this information in the context of metals. In the case of local measurements like NEXAFS, one can infer from the spectral-weight transfers whether the electrons are quantum-mechanically coherent on a length scale of order of two unit cell dimensions. Because high-T_c superconductors, like all metals, are quantal up to macroscopic scales, the usefulness of this information may be considered as questionable. However, if lattice-polaronic (or other ''localization'' effects) become important, this question gets meaningful again. Let us consider, for instance, the doped nickelates. Undoubtedly, the electrons are classical on macroscopic scales: domain wall solids or polaron lattices are formed. Mean-field calculations are well known to yield a lower bound for the polaron size, to be understood as the maximum spatial extent of the vibronic wave function. Applied to the nickelate,[7] these calculations indicate that this system is approaching the small polaron limit where the polaron fits into one unit cell: although the polaron is actually formed due to severe quantum fluctuations within the unit cell, quantum fluctuations seem unimportant on any larger scale given some reasonable temperature. At the same time, the structural data[9,10] seem to indicate that the polarons are substantially larger, implying quantal behaviour on the scale measured by the spectral-weight transfers. Hence, in principle, this issue can be *proven* by NEXAFS experiments.

The purpose of the actual study is to determine if something notable happens when comparing the NEXAFS data of cuprates and nickelates. A brief description of the experimental setup and the results obtained so far is given in Secs. II and III, respectively. By comparing spectra for $\mathbf{E}\|\mathbf{a}$ and $\mathbf{E}\|\mathbf{c}$ polarization one would naively expect that somehow large ionic motions along the **c** axis are involved in the polaron formation effect. A more quantitative analysis using a *d-d* exciton mechanism presented in Sec. IV shows that this is not necessarily the case. From the analysis of the transfer of spectral weight for LSNO as well as LSCO presented in Sec. V, we conclude that there is a substantial *dynamical* spectral-weight transfer present in both systems, showing that the polaron domain walls in LSNO are still quite quantum delocalized on length scales of the order of the x-ray wavelength (i.e., two unit cells). This is not unreasonable in the light of the rather delocalized appearance of the domain walls in the neutron scattering experiments. In Sec. VI, we summarize our results from experiment and theory.

II. EXPERIMENT

Large $La_{2-x}Sr_xNiO_{4+\delta}$ single crystals ($\sim 5\times 3\times 2$ mm^3; $x=0$, 0.1, 0.2, 0.4, and 0.6) were grown using the floating zone method as described elsewhere[20] and prepared with one surface parallel to the crystallographic (010) plane of the tetragonal unit cell. It is well known that samples with a low Sr stoichiometry ($x<0.2$) can accommodate a large amount of excess O with $0<\delta<0.2$,[1,2,21] whereas for intermediate doping ($0.2\leqslant x\leqslant 0.6$) the O concentration is very close to the correct stoichiometry. Thus in the present study the samples with $x<0.2$ were annealed together with CuO powder in vacuum sealed silica tubes at 800 °C for 30 h in order to make sure that the concentration of doped holes is controlled by the Sr stoichiometry alone for the whole sample series. All samples were then mounted on sample holders and fresh, shiny (010) surfaces were prepared using an ultramicrotome with a diamond knife.

The near-edge x-ray-absorption (NEXAFS) measurements were performed using linear polarized synchroton radiation from the AT&T Bell Laboratories Dragon beamline at the National Synchrotron Light Source. The energy resolution of the monochromator was set to ≈ 0.1 eV and ≈ 0.35 eV at the O 1*s* and Ni $2p_{3/2}$ absorption threshold, respectively. A high degree of linear polarization of $(98\pm 1)\%$ has been chosen. The O 1*s* and Ni 2*p* absorption edges of a polycrystalline NiO sample together with EELS data on the same compound were taken for the energy calibration. Bulk-sensitive spectra were recorded using a seven-element Ge array fluorescence detector, with the photon flux simultaneously monitored by the drain current from a Au mesh. In order to perform orientation-dependent measurements, the (010) surfaces of the crystals were mounted perpendicular to the incoming beam and the crystallographic **a** or **c** axis was oriented parallel to the polarization vector of the synchrotron radiation by rotating the samples around their surface normal. Therefore optical path variations hampering the direct comparison of the anisotropic spectra were eliminated. The O 1*s* raw data were corrected for self-absorption effects according to a procedure described elsewhere.[13] Finally, the spectra were normalized to absorption coefficients from standard tables[22] below and about 60–70 eV above threshold, taking into account the O stoichiometry of the samples.

III. RESULTS

In Fig. 1, we show the polarization-dependent O 1*s* absorption edges ($\mathbf{E}\|\mathbf{a}$ and $\mathbf{E}\|\mathbf{c}$) of the undoped antiferromagnetic insulators $La_2NiO_{4+\delta}$ and $La_2CuO_{4+\delta}$, respectively. The cuprate data are taken from our earlier measurements.[13] Figure 1 also displays the spectrum for polycrystalline NiO. No anisotropy is expected for the latter compound, since its crystal structure corresponds to cubic NaCl. Therefore it can be compared directly with each of the anisotropic spectra of the two other compounds. As mentioned above, the spectra are normalized between 590 and 610 eV according to their O stoichiometry. For clarity reasons, the data for NiO have been multiplied by a factor of 4. The doping-dependent spectra for $La_{2-x}Sr_xNiO_{4+\delta}$ for both polarizations are given in Fig. 2, while Fig. 3 shows the respective prepeak regions.

Dipole selection rules determine the transitions which can be realized by O 1*s* NEXAFS measurements.[23] From these, it can be anticipated that for $\mathbf{E}\|\mathbf{a}$ and $\mathbf{E}\|\mathbf{c}$ only $s\rightarrow p_x$ and $s\rightarrow p_z$ transitions are allowed, respectively. As far as the Ni

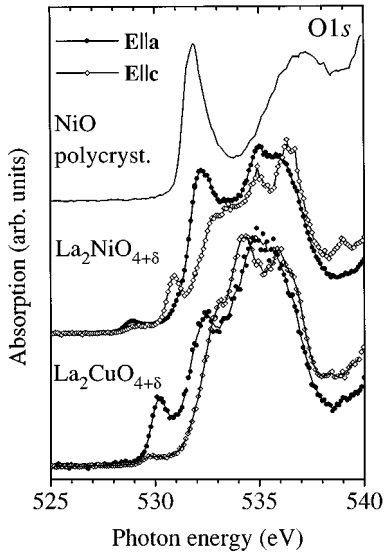

FIG. 1. Polarization-dependent O 1*s* absorption edges of single-crystalline $La_2NiO_{4+\delta}$ and $La_2CuO_{4+\delta}$ for $\mathbf{E}\|\mathbf{a}$ (solid circles) and $\mathbf{E}\|\mathbf{c}$ (open diamonds). The spectra are normalized between 590 and 610 eV according to their O stoichiometry. In addition, the O 1*s* edge of polycrystalline NiO (solid line) is shown, multiplied by a factor 4 for clarity reasons.

$2p$ absorption edges are concerned, mainly $2p \rightarrow 3d_{x^2-y^2}$ transitions are allowed for $\mathbf{E}\|\mathbf{a}$ whereas only unoccupied $3d_{3z^2-r^2}$ are probed for $\mathbf{E}\|\mathbf{c}$. Hence the symmetry of the unoccupied states under investigation can be determined from polarization-dependent experiments.

Let us first consider the spectra in Fig. 1. At photon energies above 531.5 eV one can see the so-called main edge of the O 1*s* spectra, which is determined by O $2p$ orbitals of O atoms from both within the planar La-O layers (hybridized with La $5d,4f$ states) *and* within the NiO_2 sheets (hybridized with Ni $3d$ orbitals). On the other hand, the prepeaks in the energy range below 531.5 eV have to be assigned to

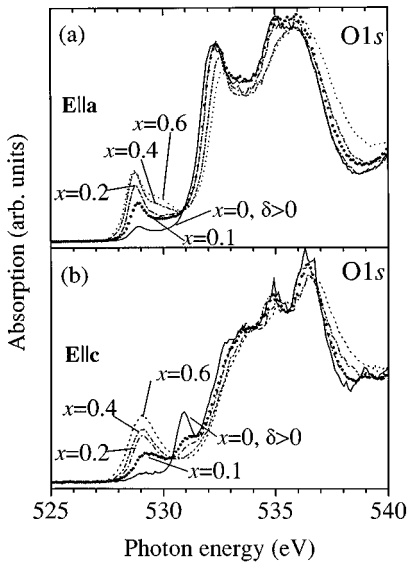

FIG. 2. Polarization-dependent O 1*s* absorption edges of *p*-type-doped $La_{2-x}Sr_xNiO_{4+\delta}$ for $\mathbf{E}\|\mathbf{a}$ (a) and $\mathbf{E}\|\mathbf{c}$ (b). The data are labeled with the Sr concentration x.

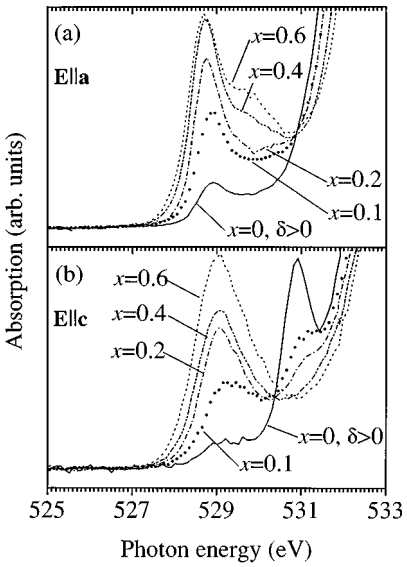

FIG. 3. Prepeak region of the O 1*s* absorption edges of $La_{2-x}Sr_xNiO_{4+\delta}$ for $\mathbf{E}\|\mathbf{a}$ (a) and $\mathbf{E}\|\mathbf{c}$ (b). The data are labeled with the Sr concentration x.

excitations within the NiO_2 layers. This is supported by results from local spin density (LSDA) band structure calculations within density functional theory[24,25] on both La_2CuO_4 and La_2NiO_4, band structure studies using self-interaction corrections (LSDA+SIC),[26,27] and further theoretical studies including on-site Coulomb and exchange interactions (LSDA+U).[28] They all predict that the states close to the Fermi level are related to the CuO_2 (NiO_2) layers only, whereas the unoccupied bands at higher energies have to be considered as a superposition of states resulting from both the CuO_2 (NiO_2) and La-O layers.

Despite the overall similarity, there are some distinct differences between the spectra for LSNO and LSCO. At about 532 eV, a strongly in-plane-polarized peak can be seen in LSNO and LSCO for $\mathbf{E}\|\mathbf{a}$ (Fig. 1), which does not change upon doping for the latter.[13] The situation is quite different in LSNO, since the corresponding peak appears to be much stronger, shifts to higher energies, and strongly decreases in intensity with increasing Sr concentration [see Fig. 2(a)]. As did Kuiper *et al.*,[29] we assign this feature in LSNO at least partly to the Ni $3d^9$ final state of the z upper Hubbard (UH) band having mainly Ni $3d_{x^2-y^2}$ character hybridized with O $2p_{x,y}$ orbitals within the NiO_2 planes. Support for the validity of this interpretation comes from (i) the strong in-plane polarization of this peak, (ii) the close coincidence of its energy position with that of the corresponding Ni $3d^9$ final state in the O 1*s* edge of NiO (see Fig. 1), and (iii) its decreasing intensity with increasing Sr concentration, reminiscent of the behavior expected for the UH band under *p*-type doping (see below). Nevertheless, since this feature is sitting on a high background, it is very difficult to determine its exact intensity and energy position. Thus there is still some ambiguity concerning the quantitative evaluation of this excitation, as will be discussed in Sec. IV. The prepeak related to the same transition into the UH band and (Cu $3d^{10}$ final state) for $La_2CuO_{4+\delta}$ is at 530.2 eV, whereas in the isotropic spectrum of NiO (Fig. 1), it appears at about 531.8 eV.

The low-energy prepeak at about 530.9 eV in the spectrum for $\mathbf{E}\|\mathbf{c}$ of $La_2NiO_{4+\delta}$ (Fig. 1) has to be assigned to the x UH band having mainly Ni $3d_{z^2-r^2}$ character hybridized with apex O $2p_z$ orbitals. This is in perfect agreement with recent LSDA+U band structure calculations by Czyzyk and Sawatzky.[28] This prepeak at 530.9 eV is much stronger than the corresponding spectral weight at 529.7 eV in $La_2CuO_{4+\delta}$, indicating the enhanced number of unoccupied states in out-of-plane apex-O $2p_z$/Ni $3d_{3z^2-r^2}$ orbitals compared to those of apex-O $2p_z$/Cu $3d_{3z^2-r^2}$ parentage in the cuprate. In analogy to results from NEXAFS measurements on $La_{2-x}Sr_xCuO_{4+\delta}$,[13,14] we have to keep in mind an O $1s$ binding energy shift between the planar and apical O sites ($\sim$0.3 eV in LSCO) which is possibly also present in the actual $La_{2-x}Sr_xNiO_{4+\delta}$ data. This would lead to an overall increase of the differences between the threshold energies in the $\mathbf{E}\|\mathbf{a}$ and $\mathbf{E}\|\mathbf{c}$ spectra, which will be of considerable importance for the discussion in Sec. IV. Since reliable experimental O $1s$ binding energies for the different O sites in $La_{2-x}Sr_xNiO_{4+\delta}$ are not available at this time, there is no clear evidence whether such a binding energy shift has also to be taken into account in the case of the nickelate.

The most pronounced changes with doping in LSNO are seen in the pre-edge features below 531 eV (see Fig. 3). For $\mathbf{E}\|\mathbf{a}$, a prepeak shows up in the former gap at about 528.7 eV which increases in intensity with increasing Sr concentration. The shape of this structure differs strongly from the corresponding prepeak in LSCO,[13,14] but is very similar to the doping-induced peak in $Li_xNi_{1-x}O$.[30] We attribute its occurrence in the annealed $La_2NiO_{4+\delta}$ sample to remaining excess O atoms and estimate their amount from a comparison of the prepeak intensity with that for $x=0.1$ and 0.2. From this, we get an amount of excess O atoms of $0.02\leqslant\delta\leqslant0.03$. Additional support for the close relationship between the intensity of this structure and the amount of excess O, δ, can be found in the recent NEXAFS studies[31] on the O $1s$ absorption edges of $La_2NiO_{4+\delta}$ with $0.00\leqslant\delta\leqslant0.12$. For $\mathbf{E}\|\mathbf{c}$, the structure at 530.9 eV decreases and shifts to higher energies, whereas a peak shows up at 529.1 eV and gets stronger with doping. A similar behavior has been found in LSCO for $\mathbf{E}\|\mathbf{c}$, but with substantially lower intensity.[13,14]

The doping dependence of the low-energy excitations for $\mathbf{E}\|\mathbf{a}$ ($\mathbf{E}\|\mathbf{c}$) in LSNO clearly exhibits the transfer of spectral weight from the the z (x) upper Hubbard band at 532 eV (530.9 eV) to the doping-induced low-energy prepeak at about 528.7 eV (529 eV) with increasing dopant concentration. This behavior is well known from the O $1s$ absorption edges of other late transition metal oxides like, e.g., LSCO or $Li_xNi_{1-x}O$. Only the transitions into the z and x upper Hubbard bands are expected to show this decreasing intensity in combination with an energy shift to higher energies under p-type doping. This gives further evidence for assigning the peak at 532 eV (530.9 eV) for $\mathbf{E}\|\mathbf{a}$ ($\mathbf{E}\|\mathbf{c}$) to the z (x) upper Hubbard band.

The intensity variations of the two NEXAFS pre-edge structures for $\mathbf{E}\|\mathbf{a}$ as a function of the Sr concentration x are shown in Fig. 4(a) together with the same kind of data from the doping-induced prepeak for $\mathbf{E}\|\mathbf{a}$ in LSCO from our earlier publication.[13] The spectral weights have been evaluated by integrating the spectral weight of the difference between

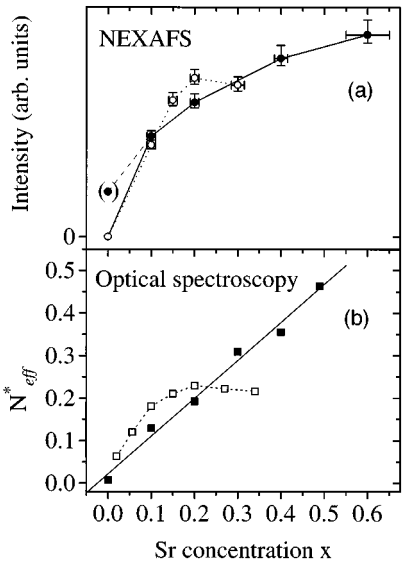

FIG. 4. Sr dependence of (a) the intensity of the doping-induced prepeaks in the O $1s$ NEXAFS spectra and (b) of the integrated low-energy spectral weight $N^*_{\mathrm{eff}}(\omega)$ from Ido *et al.* (Ref. 20) for $\mathbf{E}\|\mathbf{a}$ of $La_{2-x}Sr_xNiO_{4+\delta}$ (solid symbols) and $La_{2-x}Sr_xCuO_{4+\delta}$ (open symbols). The lines are guides to the eye.

the spectrum for $x=0$ and those with $x>0$ in both systems. The integration of the difference spectrum was performed from 525 to 530.9 eV and from 525 to 529.7 eV in the case of LSNO and LSCO, respectively. Error bars have been included in Fig. 4 in order to take into account experimental errors in the determination of the spectral weights from the O $1s$ data and in the Sr stoichiometry. Since the O $1s$ spectra of both systems were normalized to the same absorption cross section in the energy range between 590 and 610 eV far above the Fermi level, the spectral weights of the doping-induced prepeaks can be directly compared. In addition, the corresponding integrated low-energy spectral weights $N^*_{\mathrm{eff}}(\omega)$ from optical conductivity data by Ido *et al.*[20] are presented in Fig. 4(b).

From the doping dependence of the prepeak intensities in Fig. 4(a), it is obvious that the nickelate and the cuprate show a similar behavior under doping since the data from both systems exhibit almost the same absolute intensities and a substantial curvature. This is not the case for the integrated low-energy spectral weight from the optical measurements [see Fig. 4(b)], where the nickelate displays a linear doping dependence in contrast to the cuprate. The implications of these results will be discussed in Sec. V.

The occurrence of strong saturation effects in the fluorescence yield NEXAFS data and the overlap with the strong La $3d_{3/2}$ white line make the measurement of the Ni $2p_{3/2}$ absorption edge impossible. Thus one is restricted to the analysis of the Ni $2p_{1/2}$ absorption edges, which are shown for $La_2NiO_{4+\delta}$ and $La_{1.9}Sr_{0.1}NiO_{4+\delta}$ for both polarizations in Fig. 5.

IV. EXCITON SIDEBANDS AND ZHANG-RICE DOUBLETS

Let us now turn to a more detailed interpretation of the spectra. Compared to LSCO,[13,14] the prepeak region is more

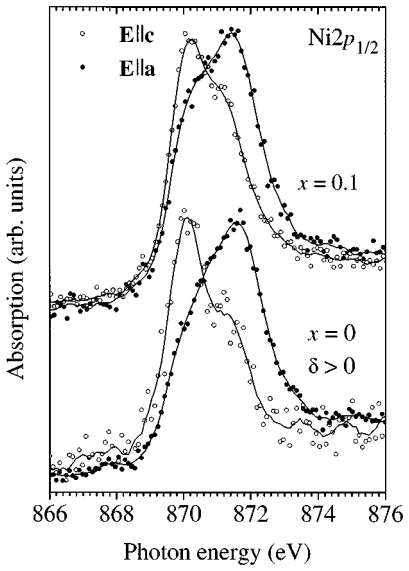

FIG. 5. Ni $2p_{1/2}$ absorption edges of $La_2NiO_{4+\delta}$ and $La_{1.9}Sr_{0.1}NiO_{4+\delta}$ for $\mathbf{E}\|\mathbf{a}$ (solid circles) and $\mathbf{E}\|\mathbf{c}$ (open circles). The data are labeled with the Sr concentration x.

complicated in the doped nickelates. For $\mathbf{E}\|\mathbf{a}$, the large band at threshold is accompanied by a high-energy shoulder. In this section we will present one possible interpretation for the structures in the prepeak region, based on theoretical observations by Zaanen and Oleś.[32] These authors showed that in cases like the nickelates the carriers are composite particles, consisting of physical holes bound to excitons. In direct analogy to phonon sidebands in the case of polarons, the removal of the physical hole releases uncompensated excitons which show up as high-energy bands in the spectral function.

Of special concern is the large intensity for $\mathbf{E}\|\mathbf{c}$ polarization, compared to that for $\mathbf{E}\|\mathbf{a}$ (see Fig. 3). This could be interpreted as indicating a lattice-polaronic dressing involving the motion of the apical oxygens toward the central Ni atom.[31] However, it is hard to imagine a mechanism stabilizing such an ''anti-Jahn-Teller'' polaron[6] in the context of the nickelates, and the observations which will be discussed in the next section seem to argue strongly against such large polaronic deformations. To resolve this issue, as well as to study the exciton sidebands, we present a calculation dealing with different aspects of p-d covalency in more detail. We find that the large **c** direction weight can be well explained by a proper choice of the apical O $2p$ level position.

The explanation of the exciton sidebands is straightforward—for a more general physical perspective on these matters we refer to the work of Zaanen and Oleś.[32] In the first instance we focus on the limit of localized d electrons. Delocalization effects will not change the picture qualitatively, as we will show later on in more detail in our discussion of the (large) p-d covalency. As a first step, we have to understand the excitations supported by the ''vacuum,'' the insulating state at half filling. Besides the spin excitations, the so-called d-d excitons are found at energies less than the charge excitation gap. These excitons are quite localized and can be described in terms of simple ligand-field theory. Introducing the notation $x\sim x^2-y^2$ and

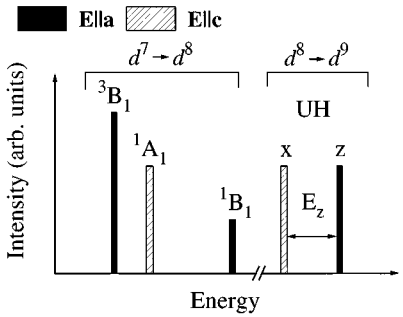

FIG. 6. Spectral function for a high-spin d^8 system with low-spin ($^2B_1$) holes without taking p-d covalency into account (solid bars: $\mathbf{E}\|\mathbf{a}$; hatched bars: $\mathbf{E}\|\mathbf{c}$; UH=upper Hubbard subband).

$z\sim 3z^2-r^2$ and neglecting the t_{2g}-like states altogether, one finds in tetragonal symmetry

$$|^3B_1(xz);1\rangle=|x\uparrow z\uparrow\rangle,$$

$$|^1B_1(xz)\rangle=\frac{1}{\sqrt{2}}(|x\uparrow z\downarrow\rangle-|x\downarrow z\uparrow\rangle),$$

$$|^1A_1(xx)\rangle=|x\uparrow x\downarrow\rangle. \tag{4.1}$$

In addition one has the $|^3B_1\rangle$ states with $M_s=0,-1$ and the highly excited (by crystal field) singlet state $|^1A_1(zz)\rangle=|z\uparrow z\downarrow\rangle$. According to ligand-field theory, these states have an energy ($E_z\sim$ tetragonal crystal field; B and C are Racah parameters)

$$E(^3B_1)=-8B+3C+E_z,$$

$$E(^1B_1)=2C+E_z,$$

$$E(^1A_1)=4B+3C+E_z[1-\sqrt{1+(4B+C)^2/E_z^2}], \tag{4.2}$$

where we have corrected $E(^1A_1)$ for the mixing with the $|^1A_1(zz)\rangle$ state, which is otherwise unimportant. The ground state of La_2NiO_4 is composed of the local high-spin states $|^3B_1\rangle$, indicating that the Hund's rule interactions overcome the crystal-field energy E_z. In the terminology of Zaanen and Oleś, the Hund's rule interactions have bound an $x\rightarrow z$ exciton to the ''noninteracting'' low-spin $|^1A_1\rangle$ state.[32] At the same time, as long as the excitation energies of the singlet states $^1B_1$ and $^1A_1$ are less than the charge excitation energy, these singlets are well defined excitations. These d-d excitons are well known and have been extensively studied in the past with optical spectroscopy.

The unoccupied density of states at half filling is rather straightforward. By removing a z hole ($\mathbf{E}\|\mathbf{c}$) from $^3B_1$ the x upper Hubbard (d^9) band is reached, while along **a** or **b** the higher-lying z UH band is reached by the removal of an x hole. The resulting d-only spectrum is given in the $d^8\rightarrow d^9$ part of Fig. 6. Comparing the experimental spectrum of NiO with those for $\mathbf{E}\|\mathbf{a}$ of undoped $La_2NiO_{4+\delta}$ and $La_2CuO_{4+\delta}$ in Fig. 1, it can be seen that the first strong peak is at 531.8 eV, 532.2 eV, and 530.2 eV, respectively. As mentioned above, the occurrence of the low-intensity fea-

tures between 528 and 530 eV in the reduced $La_2NiO_{4+\delta}$ sample has to be attributed to remaining excess O. The first strong pre-edge is due to transitions into the z UH band consisting of mainly planar Cu(Ni) $3d_{x^2-y^2}$ orbitals with some admixture of O $2p_{x,y}$ orbitals. The analogous peaks for the transitions into empty apex-O $2p_z$ orbitals hybridized with Cu(Ni) $3d_{3z^2-r^2}$ orbitals of the x UH band are at 531.8 eV in NiO and at 531 eV and 529.8 eV in the $\mathbf{E}\|\mathbf{c}$ spectra of $La_2NiO_{4+\delta}$ and $La_2CuO_{4+\delta}$, respectively. From this, it can be concluded that the separation in energy between the x and z UH bands is vanishing in the case of NiO and close to ~ 1 eV in $La_2NiO_{4+\delta}$, keeping in mind that the O $1s$ binding energy of the apical O sites is possibly about 0.3 eV lower than that for the planar O sites. In $La_2CuO_{4+\delta}$, the majority of the out-of-plane states seem to be situated below E_F, so that only a very small tail of the related density of states appears in the O $1s$ and Cu $2p$ NEXAFS spectra.[13,14] Thus the separation between the main parts of the in-plane and of the out-of-plane states in $La_2CuO_{4+\delta}$ is about 1.8–2 eV, which corresponds to the size of the charge-transfer gap.

The reason for the different splittings between the e_g orbitals ($3d_{x^2-y^2}$ and $3d_{3z^2-r^2}$) hybridized with O $2p$ orbitals of appropriate symmetry is the different size of the tetragonal Jahn-Teller distortion of the $Cu(Ni)O_6$ octahedra and the related changes in the symmetry of the crystal field at the site of the transition metal atom. It is well known from crystal structure studies that the tetragonal distortion of the $Cu(Ni)O_6$ octahedron is strongest for $La_2CuO_{4+\delta}$ and intermediate for $La_2NiO_{4+\delta}$ whereas in NiO the octahedron is undistorted. Accordingly, our measurements show that the tetragonal crystal-field splitting between x and z UH bands decreases when going from $La_2CuO_{4+\delta}$ to $La_2NiO_{4+\delta}$ and finally vanishes for NiO. A qualitative clue for the related changes within the electronic structure may be taken from LSDA band structure calculations on La_2NiO_4 by Guo and Temmerman,[25] showing that this splitting decreases with decreasing distortion in agreement with our findings. According to their analysis, this is due to a shift of the antibonding Ni $3d_{3z^2-r^2}$/apex-O $2p_z$ band to higher energies with decreasing distortion. The same trend was obtained from cluster calculations including electron-electron interactions for La_2CuO, La_2NiO_4, and K_2CuF_4.[33] As a result, the calculated symmetry of the intrinsic hole is x for La_2CuO_4, and z for K_2CuF_4, and the d^8 ground state of the nickelate corresponds to the expected $|x\uparrow z\uparrow\rangle$ Hund's rule $^3B_1$ triplet.

However, care has to be taken when trying to derive a quantitatively correct estimate for the tetragonal crystal splitting E_z from the O $1s$ spectra of undoped $La_2NiO_{4+\delta}$. As an example, Czyzyk and Sawatzky[28] pointed out that in the nickelate La $5d$-dominated conduction bands with some apex-O $2p_z$ orbital admixture extend much further down into the energy region of the x UH band than is the case for the cuprate. This could result in a rather strong hybridization of the two bands, which leads to difficulties in determining the first moment of the x UH band from the O $1s$ data. A hint for the validity of this assumption may be given by the observation that the reduction in intensity for $\mathbf{E}\|\mathbf{c}$ due to the transfer of spectral weight to the low-energy prepeak at 529.1 eV is not restricted to the structure at 531 eV but extends well into the energy region of the main edge above 531.5 eV (see Fig. 2). A more reliable way is to determine E_z from polarization-dependent measurements of the Ni $2p_{1/2}$ absorption edges as presented in Fig. 5. Only transitions into unoccupied states with $3d_{3z^2-r^2}$ character are allowed for $\mathbf{E}\|\mathbf{c}$ whereas for $\mathbf{E}\|\mathbf{a}$ predominantly empty states with $3d_{x^2-y^2}$ symmetry are probed with a small contribution from unoccupied $3d_{3z^2-r^2}$ orbitals.[23] Thus we derive a value of $\sim$1.3–1.4 eV for E_z from the energy separation between the maxima of the Ni $2p_{1/2}$ lines for the different polarization directions. Combining the information from the NEXAFS data with those from optical optical measurements,[34,20,35] a schematic picture of the electronic structure of the undoped compounds as presented in Fig. 7 can be derived. Recent LSDA+U band structure calculations[28] are in qualitative agreement with the picture shown in Fig. 7.

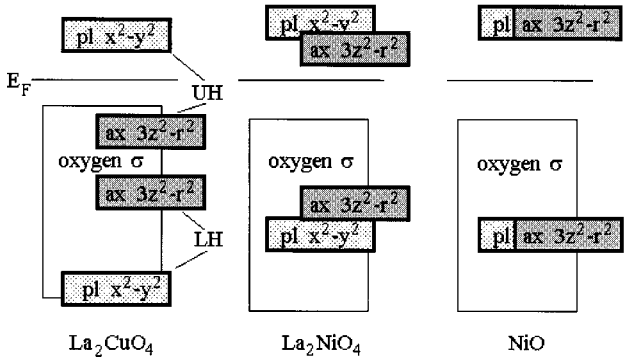

FIG. 7. Suggested electronic structure of undoped La_2CuO_4, La_2NiO_4, and NiO (pl=planar, ax=apex; LH, UH=lower, upper Hubbard subbands).

Upon hole doping, carrier states are realized with local quantum numbers which cannot be constructed from combining the quantum numbers of the added hole with the local quantum numbers characterizing the vacuum, implying binding of additional excitons to the hole. Specifically, for the nickelate it is almost sure that the lowest-lying carrier state is a doublet,

$$|^2B_1\rangle = |x\uparrow x\downarrow z\sigma\rangle. \tag{4.3}$$

High-spin states involving t_{2g} holes are ruled out by the fact that trivalent nickelates (e.g., $LaSrNiO_4$) have low-spin (doublet) character.

The lower Hubbard band part of the unoccupied density of states reveals the exciton binding. The (polarized) spectral functions in the prepeak region are calculated, using Eqs. (4.1) and (4.2),

$$\rho_{a,b}(\omega) = \sum_\sigma \langle ^2B_1|c_{x\sigma}\delta(\omega - H + E(^3B_1))c^\dagger_{x\sigma}|^2B_1\rangle$$

$$= \frac{3}{2}\delta(\omega) + \frac{1}{2}\delta(\omega - \Delta E(^1B_1)),$$

$$\rho_c(\omega) = \sum_\sigma \langle ^2B_1|c_{z\sigma}\delta(\omega - H + E(^3B_1))c^\dagger_{z\sigma}|^2B_1\rangle$$

$$= \delta(\omega - \Delta E(^1A_1)), \tag{4.4}$$

where the energies of the excitons are relative to the ($^3B_1$) ground state energies, while the weight vectors follow from fractional parentage, which is easy to calculate. The structure

of the prepeak region in the experiment resembles this result (Figs. 3 and 6). For $\mathbf{E}\|\mathbf{a}$, the large threshold peak (no excitons excited) is accompanied by a much smaller satellite, corresponding with the shake-off of an *xz* singlet exciton. The peak for $\mathbf{E}\|\mathbf{c}$ is shifted to higher energies compared to the $\mathbf{E}\|\mathbf{a}$ threshold peak by an amount corresponding to the energy difference between the high- and low-spin states of the whole system.

Let us now turn to the effects of *p*-*d* covalency. This is obviously important since the excitations mentioned above are probed via the O $2p$ character, modifying especially the spectral weight distributions. We have addressed these matters by a model calculation of the standard cluster variety.[36–38] To keep this calculation as simple as possible, we have introduced two justifiable additional simplifications.

(i) We have followed the spirit of multiband Hubbard models, including a full treatment of the Coulomb and exchange interactions between the e_g (x,z) $3d$ electrons. The t_{2g} electrons have been neglected altogether, while the *p*-*d* and *p*-*p* Coulomb/exchange interactions are neglected as well.

(ii) We limit ourselves to a single NiO_6^{4-} cluster. It can be argued that the use of such a cluster can be dangerous if one wants to address spectroscopic information involving the $2p$ electrons: for the cuprates one needs at least a cluster containing two metal ions.[11,17] However, it is well established that nickelates are of the intermediate (in between Mott-Hubbard and charge-transfer) variety in the Zaanen-Sawatzky-Allen phase diagram.[39,37] Accordingly, the carriers in the nickelates are much more localized (in the sense of the Zhang-Rice mapping[8]) than the holes in the cuprates. The effects of delocalization in the lattice on the strong *p*-*d* hybrid states of the clusters are therefore expected to be rather insignificant.[18] We notice that these statements imply that the $2p$-$3d$ hybrid states obey the same symmetry rules as the pure states, so that the basic structure of the excitonic spectrum is unaltered compared to the *d*-only case we just discussed (see Fig. 6).

This calculation is standard[37] and too lengthy to be reproduced in full detail. Let us outline the procedure, paying attention to the steps which are not immediately obvious. A cluster is considered of a Ni ion with $3d_{x^2-y^2}$ ($d^\dagger_{x\sigma}$) and $3d_{z^2-r^2}$ ($d^\dagger_{z\sigma}$) orbitals, surrounded by four ''planar'' oxygens with (σ) $2p$ orbitals ($p^\dagger_{1\sigma},\ldots,p^\dagger_{4\sigma}$, where σ as a subscript indicates the spin direction) and two apical oxygens with $2p$ orbitals $p^\dagger_{5\sigma}$ and $p^\dagger_{6\sigma}$. The bonding (with respect to the Ni states) symmetrized *p* states are

$$p^\dagger_{z1\sigma}=\frac{1}{\sqrt{2}}(p^\dagger_{5\sigma}+p^\dagger_{6\sigma}),$$

$$p^\dagger_{x\sigma}=\frac{1}{2}(p^\dagger_{1\sigma}-p^\dagger_{2\sigma}+p^\dagger_{3\sigma}-p^\dagger_{4\sigma}),$$

$$p^\dagger_{z2\sigma}=\frac{1}{2}(p^\dagger_{1\sigma}+p^\dagger_{2\sigma}+p^\dagger_{3\sigma}+p^\dagger_{4\sigma}), \tag{4.5}$$

and the orthogonal nonbonding states, unoccupied with holes in the ground state,

$$\tilde{p}^\dagger_{z1\sigma}=\frac{1}{\sqrt{2}}(p^\dagger_{5\sigma}-p^\dagger_{6\sigma}),$$

$$\tilde{p}^\dagger_{x\sigma}=\frac{1}{2}(p^\dagger_{1\sigma}-p^\dagger_{2\sigma}-p^\dagger_{3\sigma}+p^\dagger_{4\sigma}),$$

$$\tilde{p}^\dagger_{z2\sigma}=\frac{1}{2}(p^\dagger_{1\sigma}+p^\dagger_{2\sigma}-p^\dagger_{3\sigma}-p^\dagger_{4\sigma}). \tag{4.6}$$

The transfer matrix elements are, in terms of the V^σ_{pd} in planar (**ab**) and perpendicular (**c**) directions,

$$t_x=\langle d_x|H|p_x\rangle=V^\sigma_{pd}(ab),$$

$$t_{z1}=\langle d_z|H|p_{z1}\rangle=\sqrt{2}V^\sigma_{pd}(c),$$

$$t_{z2}=\langle d_z|H|p_{z2}\rangle=\frac{\sqrt{3}}{2}V^\sigma_{pd}(ab),$$

with all other transfer matrix elements zero by symmetry.

The local, unoccupied $2p$ state densities in the **a** (or **b**) and the **c** directions are calculated from (E_0 is the ground state energy)

$$\rho_a(\omega)=\sum_\sigma \langle 0|p_{1\sigma}\delta(\omega-H+E_0)p^\dagger_{1\sigma}|0\rangle,$$

$$\rho_c(\omega)=2\sum_\sigma \langle 0|p_{5\sigma}\delta(\omega-H+E_0)p^\dagger_{5\sigma}|0\rangle, \tag{4.7}$$

with the factor of 2 in the expression for ρ_c because there are twice as many O atoms in the **c** direction per unit cell as along the **a** direction. Inverting Eqs. (4.5) and (4.6) and using that the nonbonding states Eq. (4.6) are fully occupied with electrons,

$$\rho_a(\omega)=\frac{1}{4}\sum_\sigma \langle 0|(p_{x\sigma}+p_{z2\sigma})\delta(\omega-H+E_0)\times(p^\dagger_{x\sigma}+p^\dagger_{z2\sigma})|0\rangle,$$

$$\rho_c(\omega)=\sum_\sigma \langle 0|p_{z1\sigma}\delta(\omega-H+E_0)p^\dagger_{z1\sigma}|0\rangle. \tag{4.8}$$

The $z2$ occupancy (planar O $3z^2-1$ character) will be almost negligible in the ground state. In other words, the **a**-axis spectral weight is a factor ~ 2 smaller than one would expect from stoichiometry alone. This is a nontrivial correlation effect. Because of the Zhang-Rice mapping, we forced the $2p$ states to obey the point group symmetries of the $3d$ states centered on the Ni ion. This reasoning is valid only if the binding energy of the Zhang-Rice doublet is much larger than its delocalization energy, an assumption which becomes questionable in the case of, e.g., cuprates, while it should be unproblematic for the nickelates. Hence, because of this nontriviality the **c**-axis weight problem is only half as severe as one would think naively. This will turn out, however, to be insufficient to explain all of the huge **c**-axis spectral weight.

To calculate the upper Hubbard band, the spectral functions are calculated with regard to the divalent $^3B_1$ ground state which is calculated in the basis of d^8 and $d^9\underline{p}$ configu-

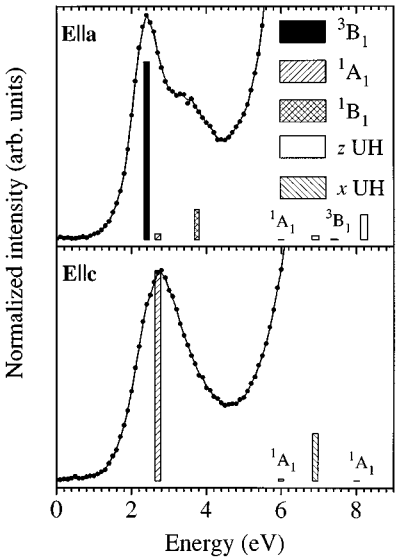

FIG. 8. Spectral function for a high-spin d^8 system with low-spin ($^2B_1$) holes including p-d covalency. The experimental O 1s spectra of $La_{1.4}Sr_{0.6}NiO_{4+\delta}$ for both polarizations have been normalized by a *common* factor to match the intensity of the calculated $^1A_1$ final state (z UH, x UH: z and x upper Hubbard band, respectively).

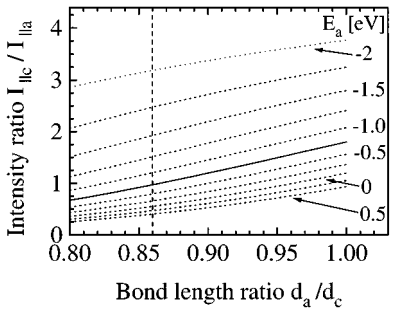

FIG. 9. Calculated intensity ratio $I_{\|\mathbf{c}}/I_{\|\mathbf{a}}$ for the $^1A_1$ and $^3B_1$ final states as a function of the in-plane to out-of-plane O-Ni bond length ratio d_a/d_c with E_a as parameter. The dashed vertical line corresponds to the O-Ni bond length ratio of the undoped $La_2NiO_{4+\delta}$ (see text).

rations. The one-hole states making up the upper Hubbard band are the d^9 x and z states, where the hybridization with the high-lying[38] $d^{10}\underline{p}$ configurations (where $\underline{p}$ denotes an O $2p$ ligand hole) is neglected. The prepeak, or lower Hubbard band, is calculated using the three-hole ground state with $^2B_1$ symmetry for the vacuum in Eq. (4.8). We include, besides the d^7 state Eq. (4.3), the $d^8\underline{p}$ and $d^9\underline{pp'}$ states. Because of the low D_{4h} symmetry this amounts to solving a 15×15 problem. The interactions are parametrized as follows:[38] $3d$ monopole Coulomb interaction U (or Racah A) and charge-transfer energy (Δ), such that $d^9\underline{p}$ is at Δ relative to d^8, while d^7 is at $U-\Delta$ and $d^9\underline{pp'}$ at $\bar{\Delta}$ relative to $d^8\underline{p}$. In addition, we include the Racah parameters B and C for the $3d$ multipole/exchange interactions, a $3d$ tetragonal crystal-field parameter E_z, and a parameter E_a describing the position of the apical oxygen level ($z1$) relative to that of planar oxygens. The outcomes barely depend on the relative positioning of the planar (x,$z2$) p levels, and we have taken their splitting to be of the order of the $2p$ bandwidth (4 eV, with the $3z^2-1$ level at the bottom of the band). Upon addition of an electron to this three-particle carrier state, the two-hole states of $^3B_1$, $^1B_1$, and $^1A_1$ symmetry are reached as in the simple d-only case. They are calculated following the same procedure as for the two-hole ground state, the $^3B_1$,$^1B_1$, and $^1A_1$ final states representing 4×4 and $^1A_1\sim5\times5$ problems, respectively. The parameters which have been used in the actual calculations are taken as in NiO:[38] $U=7.0$ eV, $B=0.1$ eV, $C=0.387$ eV, $\Delta=6.0$ eV, $E_z=1.3$ eV, $E_a=-0.75$ eV, $E_{z2}=4.0$ eV, $t_x=2.0$ eV, and the in-plane to out-of-plane Ni-O bond length ratio $d_{ab}/d_c=0.86$.

The outcomes are summarized in Figs. 8 and 9. The overall shape of the spectral function shown together with the O 1s spectra of $La_{1.4}Sr_{0.6}NiO_{4+\delta}$ in Fig. 8 is quite similar to the d-only spectrum of Fig. 6. Of the 13 two-hole final states, three dominate the spectrum corresponding to the ground states in the different symmetry sectors ($^3B_1$ threshold and $^1B_1$ shoulder in the **a** direction, $^1A_1$ threshold in the **c** direction). The experimental data for both polarization directions have been normalized by a *common* factor in order to match the intensity of the $^1A_1$ final state for $\mathbf{E}\|\mathbf{c}$. The spectra have also been shifted by the same energy in order to match the energy position of the $^1A_1$ final state.

There is good agreement between theory and experiment in the energy region of the doping-induced prepeaks. However, at first glance there seems to be a discrepancy between the theoretical band gap between the x UH band and the lowest $^3B_1$ prepeak of about 4.5 eV and the corresponding experimental separation between the lowest doping-induced prepeak for $\mathbf{E}\|\mathbf{a}$ and the prepeak in the undoped $La_2NiO_{4+\delta}$for $\mathbf{E}\|\mathbf{c}$ (see Fig. 2) of the order of 2.5 eV. There are two effects which help in solving this problem. First, we have to keep in mind that band formation effects should reduce the 4.5 eV value from our cluster calculations by ~1 eV. Furthermore, as we argued above, there is strong evidence for the experimental first moment of the x UH band being shifted to higher energies by about 1 eV compared to the position of the prepeak for $\mathbf{E}\|\mathbf{c}$ in undoped $La_2NiO_{4+\delta}$, due to the hybridization between the x UH band and low-lying La-O conduction bands. Thus both approaches converge toward a band gap of about 3.5–4 eV in agreement with results from optical spectroscopy,[35] confirming our choice of parameters Δ, U, and t_x listed above as the same as for NiO.[38]

Let us now consider the mechanisms influencing the large spectral weight in the **c** direction in both the experimental and theoretical data of the doped compound (see Figs. 3 and 8). The **c**- vs **a**-axis intensity ratio is in the first instance governed by the net hole occupancy of the apical O $2p_z$ level, relative to that of the planar O $2p_{x^2-y^2}$ states. It is clear that the apical O $2p_z$ level hole occupation will increase if the in-plane to out-of-plane O-Ni bond length ratio increases because of the enhanced apex-O p_z–Ni $3d_{3z^2-r^2}$ hybridization. These ratios are related to each other according to[40]

$$\frac{V_{pd}^{\sigma}(c)}{V_{pd}^{\sigma}(ab)}=\left(\frac{d_{ab}}{d_c}\right)^{7/2}. \tag{4.9}$$

This explains the rise of the **c**- vs **a**-axis intensity ratio with the increasing in-plane to out-of-plane bond length ratio as given in Fig. 9. Second, we found that the intensity ratio is a very sensitive function of the position of the apical $2p_z$ level, relative to that of the $2p_{x^2-y^2}$ planar level, as can be seen from the strong influence of E_a on $I_{\|\mathbf{c}}/I_{\|\mathbf{a}}$ in Fig. 9. Hence, keeping the O-Ni bond length ratio fixed at its value of 0.86 at half filling (dashed line in Fig. 9), we only need a shift $E_a \sim -0.75$ eV towards E_F of the apical oxygen level. In fact, LDA calculations indicate that at least the bare apical O level in La_2CuO_4 indeed lies closer to E_F by an amount ~ 2 eV.[41] Although further calculations are needed to get a more direct comparison with our O level positions, which are corrected for *p-p* hybridization, this explanation of the large **c**-axis intensity appears to us as much more likely than invoking large anti-Jahn-Teller polaronic effects.[31] We note, however, that some (uniform) contractions of the apical O-Ni bond do happen as a function of increasing Sr content,[1,2] which might contribute to the enhanced **c**-axis intensity at larger dopings.

The most serious problem with the present interpretation lies in the position of the $xz(S)$ ($^1B_1$) exciton side band. The $^1B_1$ exciton energy is rather weakly influenced by the tetragonal distortion, and taking into account that in other regards La_2NiO_4 is expected to be quite similar to NiO, we can use optical data of the latter to obtain an estimate $\simeq 2.75$ eV for the $^1B_1$ exciton energy.[34] This is close to twice as large as the actual energy difference between the $^3B_1$ peak and the $^1B_1$ sideband of about 1.3 eV in our experimental spectra for $\mathbf{E}\|\mathbf{a}$ (see Fig. 8). This forced us to reduce the values of the Racah exchange parameters by $\sim 30\%$ in our calculations ($B=0.1$ eV, $C=0.387$ eV) instead of using the numbers determined by optical spectoscopy on NiO ($B=0.13$ eV, $C=0.6$ eV). Assuming that our assignment is correct, this indicates a rather strong covalent reduction of these parameters, in fact a much stronger reduction than deduced from the expected ionicity of this Ni compound. Covalent admixture will have a similar reducing effect on the magnitude of the ground state magnetic moment. Interestingly, Kaplan *et al.*[42] found an anomalously small magnetic moment in the nickelate from their analysis of the neutron scattering form factor. These authors put forward an alternative explanation for this moment reduction. Recently it was shown that local fluctuations involving low-spin $^1A_1$ states can also lead to a reduction of the local moments.[43,42] For this to happen, the system has to be close to the high-spin–low-spin transition. These fluctuations are driven by the superexchange interaction, while they have to overcome the $^1A_1$ exciton energy. We already pointed out in the beginning of this section that the vicinity to the high-spin–low-spin transition is in fact measured in our experiment by the relative peak position of the $^1A_1$ ($\mathbf{E}\|\mathbf{c}$) compared to $^3B_1$ ($\mathbf{E}\|\mathbf{a}$) line. The experimental separation between the $^3B_1$ and the $^1A_1$ final states corresponding to the low-spin exciton energy amounts to $\simeq 0.3$ eV. However, this number could be increased up to $\simeq 0.6$ eV when taking into account an eventual O 1*s* binding energy shift between planar and apical O sites of $\sim$ 0.3 eV. In the calculations, this excitation energy is mostly tuned by E_z, requiring $E_z=1.3$ eV in agreement with the estimate from the splitting between the peak positions of the excitonic Ni $2p_{1/2}$ lines for the different polarizations. This is rather large compared to the superexchange interaction $J\approx 0.03$ eV determined from polarized Raman scattering measurements.[44] Together with the fact that these low-spin–high-spin fluctuation will not change the $^1B_1$ energy, this explanation appears to us as less likely. Further experiments (e.g., optical absorption at half filling) are needed to come to a final conclusion.

V. DYNAMICAL SPECTRAL WEIGHT TRANSFER AND COHERENT POLARON HOPPING

The interesting thing about the data presented in Fig. 4 is the similarity between the doping dependence of the NEXAFS prepeak intensities in the cuprate and the nickelate, whereas the results on the integrated low-energy spectral weight from optical spectroscopy for these two systems are obviously quite different from each other. Several articles dealing with high-energy[12,45,14,13] and optical spectroscopy[35,20] on LSCO have been published so far, all of them giving evidence for a nonlinear increase of the doping-induced structures at lower energies. In the case of NEXAFS this increase can be divided into a static (intracell) and a dynamical (intercell) part, the former yielding a linear growth with doping whereas the latter gives a nonlinear contribution.[15,18,17] Since due to a positive feedback between electron-phonon interaction and Zhang-Rice localization[8] polarons and, furthermore, polaron structures are formed in the case of LSNO, a suppression of the dynamical transfer of spectral weight could be expected in this compound if these polarons have to be considered as small. From the analysis of the LSNO data, we will show that this system is *not* in the small polaron regime. Thus there seems to be a substantial overlap between these local lattice distortions even for lower dopings.

To illustrate the physics behind the transfer of spectral weight effects, let us consider a two-site Hubbard model originally suggested by Sawatzky,[46] characterized by a Coulomb interaction $U \gg t$, where t denotes the transfer matrix element. First consider half filling, with one electron on each site. Clearly, there is an equal number of ways to add or remove an electron (one per site) and the added electron always doubly occupies a site, costing an energy $\sim U$. Hence we find an upper (UH) and lower (LH) Hubbard band, separated by U, with equal spectral weights ~ 1. Let us now consider the situation where we have doped one additional hole. The spin 1/2 ground state wave function is trivial (l,r indicate the left and right sites),

$$|\phi_0\rangle = \frac{1}{\sqrt{2}}(c^\dagger_{l\uparrow} - c^\dagger_{r\uparrow})|\mathrm{vac}\rangle, \tag{5.1}$$

taking a positive t. Mimicking NEXAFS, we want to know the spectral function of adding an electron at, say, the right site,

$$A(\omega) = \sum_\sigma \langle \phi_0 | c_{r\sigma}\delta(\omega - H)c^\dagger_{r\sigma}|\phi_0\rangle$$

$$= \sum_{j\sigma} |\langle j|c^\dagger_{r\sigma}|\rangle|^2 \delta(\omega - E_j), \tag{5.2}$$

where j is the jth eigenstate, at energy E_j, of the two-electron problem. To keep matters as simple as possible, we

neglect half of the Hilbert space and consider only the three states directly reached by adding an electron on the right site—the remainder of the Hilbert space does not matter as long as we are not interested in the internal structure of the Hubbard bands. Hence we have the (triplet) eigenstate reached by adding an up electron,

$$|3\rangle = c_{l\uparrow}^{\dagger} c_{r\uparrow}^{\dagger} |\mathrm{vac}\rangle, \tag{5.3}$$

as well as the $M_s = 0$ states reached by adding the down electron,

$$|0\rangle = c_{l\uparrow}^{\dagger} c_{r\downarrow}^{\dagger} |\mathrm{vac}\rangle,$$

$$|U\rangle = c_{r\uparrow}^{\dagger} c_{r\downarrow}^{\dagger} |\mathrm{vac}\rangle. \tag{5.4}$$

The latter two states are connected by hopping and because $t/U \ll 1$ the eigenstates are

$$|1\rangle = |0\rangle - \frac{t}{U}|U\rangle,$$

$$|2\rangle = |U\rangle + \frac{t}{U}|0\rangle. \tag{5.5}$$

State $|1\rangle$ is (like $|3\rangle$) a LH state at $E \simeq 0$, and $|2\rangle$ is an UH state at $\simeq U$, both corrected for their mutual hybridization.

Filling in states $|1\rangle$–$|3\rangle$ in Eq. (5.2) for the spectral function yields to lowest order in t/U

$$A(\omega) = \left(1 + \frac{|t|}{U}\right)\delta(\omega) + \left(\frac{1}{2} - \frac{|t|}{U}\right)\delta(\omega - U), \tag{5.6}$$

the two terms representing the unoccupied part (by doping) of the lower Hubbard band, and the upper Hubbard band, respectively.

Compared to band insulators, Eq. (5.6) is rather odd. In the noninteracting case, the number of states in the conduction and valence bands would be fixed and the relative weights would be 1/2 for the unoccupied part of the valence band and 1 for the conduction band. First consider $t/U \to 0$. In this limit we find weights ~ 1 and 1/2 for the LH and UH bands respectively, exactly opposite to the band limit. This is in fact a triviality occurring in the simple electrostatics problem corresponding to the classical ($t = 0$) limit of the Hubbard model: there is no way of feeling the on-site Coulomb energy U for the added electron, if the site it reaches is empty. Hence, every doped hole removes a state from the upper Hubbard band and adds it to the unoccupied part of the lower Hubbard band. For the extended system, the UH weight $\sim 1 - x$ per site while the LH grows $\sim 2x$ per site, twice as fast as expected from doping alone.

In addition, Eq. (5.6) indicates that a finite t increases the weight of the low-energy spectral weight further, relative to the weight of the upper Hubbard band, by amounts $\sim t/U$. This so-called dynamical spectral-weight transfer effect yields more interesting information: the spectral weights measure the degree of quantum coherence on short length scales in the ground state. This is easily deduced from the above toy model. The phasing of the low-lying state $|1\rangle$ is similar to that of the ground state and the phasing of the high-lying state $|2\rangle$ is opposite. This is a rather general property of wave functions: the low-lying states are bondinglike, like the ground state, and the high-lying states have to be orthogonal. Therefore constructive interference is found at low energies, and destructive interference at high energies.

The full theory is controlled by the parameter t/U. If this parameter is small, the physics remains local and the above toy model is representative. The integrated weights for the lower and upper Hubbard bands of extended systems turn out to be, to first order,[16,19]

$$A_{\mathrm{LH}}(x) = 2x + 2\frac{|t|}{NU}\sum_{i\boldsymbol{\delta}\sigma} \langle c_{i,\sigma}^{\dagger} c_{i+\boldsymbol{\delta},\sigma}\rangle,$$

$$A_{\mathrm{UH}}(x) = 1 - x - 2\frac{|t|}{NU}\sum_{i\boldsymbol{\delta}\sigma} \langle c_{i\sigma}^{\dagger} c_{i+\boldsymbol{\delta},\sigma}\rangle, \tag{5.7}$$

where N is the number of sites. The local (or bond) kinetic energy $\langle c_i^{\dagger} c_{i+\delta}\rangle$ measures the quantum coherence around the site i, and has to be calculated from the true many-particle ground state. In this regard, a major simplification is achieved in the toy problem [with Eq. (5.1), $\langle c_l^{\dagger} c_r\rangle = 1$].

Let us now reconsider the above in the presence of large electron-phonon couplings and low carrier densities, and ask what happens with the spectral-weight transfers if small polarons are formed. One first considers the electron-phonon bound state formed if the electron is localized, and the delocalization (hopping) is taken into account perturbatively. In more detail,[47] consider the electron-phonon Hamiltonian,

$$H_{e-\mathrm{ph}} = t\sum_{i\boldsymbol{\delta}\sigma} c_{i+\boldsymbol{\delta},\sigma}^{\dagger} c_{i\sigma} + \sum_{\mathbf{q}} \omega_{\mathbf{q}} a_{\mathbf{q}}^{\dagger} a_{\mathbf{q}} + \sum_{i\mathbf{q}\sigma} c_{i\sigma}^{\dagger} c_{i\sigma} e^{i\mathbf{q}\cdot\mathbf{R}_i} M_{\mathbf{q}} (a_{\mathbf{q}} + a_{-\mathbf{q}}^{\dagger}), \tag{5.8}$$

assuming as before a single relevant electronic state per unit cell, with a local (Holstein) coupling to a phonon bath. The system Eq. (5.8) is transformed using the ''displaced phonon'' canonical transformation, which would yield the exact answer if $t = 0$,

$$H'_{e-\mathrm{ph}} = e^{S} H e^{-S},$$

$$S = -\sum_{i\mathbf{q}\sigma} n_{i\sigma} e^{i\mathbf{q}\cdot\mathbf{R}_i} \frac{M_{\mathbf{q}}}{\omega_{\mathbf{q}}} (a_{\mathbf{q}} - a_{-\mathbf{q}}^{\dagger}),$$

$$H'_{e-\mathrm{ph}} = \sum_{\mathbf{q}} \omega_{\mathbf{q}} a_{\mathbf{q}}^{\dagger} a_{\mathbf{q}} - E_{\mathrm{pol}} \sum_{i} n_{i\sigma} + t\sum_{i\boldsymbol{\delta}\sigma} c_{i+\boldsymbol{\delta},\sigma}^{\dagger} c_{i\sigma} X_{i+\boldsymbol{\delta}}^{\dagger} X_i . \tag{5.9}$$

Hence we have fully relaxed the lattice around the electron, yielding a polaron binding energy $E_{\mathrm{pol}} = \Sigma_{\mathbf{q}} M_{\mathbf{q}}^2/\omega_{\mathbf{q}}$, at the expense of introducing a complicated multiphonon process in the hopping,

$$X_i=\exp\left[\sum_q e^{i\mathbf{q}\cdot\mathbf{R}_i}\frac{M_\mathbf{q}}{\omega_\mathbf{q}}(a_\mathbf{q}-a^\dagger_{-\mathbf{q}})\right], \tag{5.10}$$

expressing the fact that the full dressing cloud has to be pulled around in the hopping process. The dressed hopping term in H' is the source of the formidable difficulties of small polaron theory, which can only be handled in some limiting cases.

Let us now return to the issue of the spectral-weight transfers. Although at first sight, we seem to complicate matters further by adding a Hubbard term $U/2\Sigma_{i\sigma}n_{i\sigma}n_{i-\sigma}$ to Eq. (5.8), the ramifications with respect to the spectral-weight transfer are simple. The point is that the relevant physical limit amounts to $U\gg E_{\rm pol}$: the time scale for the fluctuations involving the upper Hubbard band is much shorter than the relaxation time relevant for the polaron formation process. In other words, the phonon dressing in the ground state can be considered as frozen on the time scales involved in the determination of the spectral weights. In terms of the toy model, the doubly occupied state $c^\dagger_{r\uparrow}c^\dagger_{r\downarrow}|\text{vac}\rangle$, for instance, should have as much phonon dressing as the state $c^\dagger_{r\uparrow}|\text{vac}\rangle$ if one wants to determine the lowest moments of the spectrum. Technically, one has first to integrate out the fast fluctuations involving the upper Hubbard band, using the canonical transformations of Harris and Lange,[16] and subsequently the (slow) phonon fluctuations using Eq. (5.9).[48] One finds

$$A_{\rm LH}(x)=2x+2\frac{|t|}{NU}\sum_{i,\boldsymbol{\delta},\sigma}\langle c^\dagger_{i\sigma}c_{i+\boldsymbol{\delta}\sigma}X^\dagger_{i+\boldsymbol{\delta}}X_i\rangle,$$

$$A_{\rm UH}(x)=1-x-2\frac{|t|}{NU}\sum_{i,\boldsymbol{\delta},\sigma}\langle c^\dagger_{i\sigma}c_{i+\boldsymbol{\delta}\sigma}X^\dagger_{i+\boldsymbol{\delta}}X_i\rangle, \tag{5.11}$$

with the X's as given by Eq. (5.10). This is the central result of this section. It states that by studying the spectral weights, information is obtained about a central quantity in small polaron theory, the renormalized bond kinetic energy $\sim\langle c^\dagger_i c_{i+\delta}X^\dagger_i X_{i+\delta}\rangle$. In the ''classic'' small polaron theory it is assumed that macroscopic properties like transport can be directly inferred from the renormalizations on the shortest length scales as described by Eqs. (5.9) and (5.10). The significance of Eq. (10) is that this assertion can be tested directly, and we will see that the situation in the nickelates is quite likely more complicated.

Equation (5.11) is within the limitations of the model assumptions a rigorous result. The problem is that the quantity $\langle c^\dagger_{i+\delta}c_iX_{i+\delta}X_i\rangle$ has to be calculated as an expectation value with regard to the full many-body ground state. Even in the absence of electron-phonon coupling this is a formidable task which cannot be executed except in some exceptional cases where the ground state is known.[19] However, some limiting cases can be studied and in the present context the small polaron limit is of interest, which is straightforward to derive. The small polaron limit is defined by demanding that the bare hopping $t\ll E_{\rm pol}$ in Eq. (5.9). In lowest order, one can neglect the mixing of states in the Hilbert space having different phonon occupations, and taking the expectation values one derives[47]

$$\langle c^\dagger_{i+\boldsymbol{\delta},\sigma}c_{i\sigma}X^\dagger_{i+\boldsymbol{\delta}}X_i\rangle=t\,\exp\left[\sum_\mathbf{q}\frac{M^2_\mathbf{q}}{\omega_\mathbf{q}}[1-\cos(\mathbf{q}\cdot\boldsymbol{\delta})]\times(2N_\mathbf{q}+1)\right], \tag{5.12}$$

or roughly

$$\langle c^\dagger_{i+\delta,\sigma}c_{i\sigma}X^\dagger_{i+\delta}X_i\rangle\simeq t\,\exp(-\alpha^2),\quad k_BT\ll\omega_0$$
$$\simeq t\,\exp\left(-\alpha^2\frac{k_BT}{\omega_0}\right),\quad k_BT>\omega_0, \tag{5.13}$$

where ω_0 is the Debye frequency and $\alpha^2\simeq E_{\rm pol}/\omega_0$ the average number of phonons bound to the electron. In other words, at zero temperature the bare hopping gets reduced by a mass enhancement factor which is exponential in the number of phonons bound to the polaron. At temperatures of order of the Debye temperature, real phonons start to proliferate, dephasing the coherent polaron motion and adding a further exponential dependence on temperature. The ramifications for the spectral-weight transfer are obvious: substantial phonon dressings would lead to a strong suppression of the dynamical effect already at zero temperature and the remnants of the dynamical effect would disappear quickly with rising temperature.

The preceding discussion is valid in the limit of infinitely small hole density, and matters get further complicated at finite densities. In the nickelate we are helped by the knowledge that the holes form classically ordered structures, like domain walls and polaron lattices. In zeroth order we can think of the polarons as classical objects occupying separate regions in space. However, every polaron will behave quantum mechanically in a finite region of space around its average position and if the interparticle spacing becomes less than this coherence length, one expects deviations of the monotonic increase of the spectral-weight transfer with particle density, as expected for nonoverlapping holes. Generically, these overlap effects will cause a positive curvature to the density dependence of the dynamical spectral-weight transfer. The neighboring hole will act to increase the quantum fluctuations of the hole under consideration, thereby increasing the bond kinetic energy—at the end one has to approach a quantum limit such as, for instance, the Fermi liquid. We notice that this behavior is rather nicely illustrated for calculations of the spectral weight transfers of (quantum dominated) Hubbard models, where one always finds these curvatures.[17,19] As we will now demonstrate, the qualitative behavior of the spectral-weight transfers as a function of doping is more easily studied experimentally than the absolute magnitudes needed to decide on the behavior of a single hole.

Let us consider the intensity of the doping-induced prepeaks in the NEXAFS spectra of LSCO and LSNO for $\mathbf{E}\|\mathbf{a}$ as a function of the Sr concentration x as shown in Fig. 4(a). The data point at $x=0$ for $La_2NiO_{4+\delta}$ has to be neglected since the remaining intensity in the prepeak region of the undoped sample is undoubtedly due to remaining excess O in that sample. This is supported by NEXAFS studies on

$La_2NiO_{4+\delta}$ with $0.00 \leqslant \delta \leqslant 0.12$,[31] where the intensity of the prepeak for $\delta = 0.00$ was found to be much lower compared to that in the O 1*s* data of the actual $La_2NiO_{4+\delta}$ sample with an estimated excess O stoichiometry of $0.02 \leqslant \delta \leqslant 0.03$ (see Figs. 2 and 3). Analogous changes in the O 1*s* data of $La_2CuO_{4+\delta}$ as a function of δ can be found in Ref. 12. Thus the data point for an effectively undoped sample (i.e., $x=0$ and $\delta=0$) has obviously to be set to zero intensity as has been done in Fig. 4(a).

The shapes of the curves for LSNO and LSCO are similar in their common doping range, both exhibiting a distinct deviation from the linear increase expected from the localized limit ($t=0$) behavior.[15,18] This indicates that there is a significant dynamical contribution to the transfer of spectral weight in both compounds.

Comparing the prepeak intensities from the NEXAFS data with the respective $N^*_{\mathrm{eff}}(\omega)$ in Fig. 4(b), it appears that the corresponding curves for LSCO show similar behavior in both experiments. Interestingly, this seems not to be the case for LSNO, since the optical data follow a more or less straight line, whereas as stated above the NEXAFS data exhibit a significant curvature. The reason for this discrepancy between the optical and the NEXAFS measurements on insulating LSNO is possibly due to the different length scales probed in the experiments in connection with the quantum coherence length between the polarons in this compound. From the fact that the dynamic transfer only shows up in the NEXAFS data, we assert that there is a quantum coherence between the sites of neighboring polarons on the length scale of a lattice constant, whereas on the scale probed by optical measurements the polarons appear as classical objects. This results in the disappearance of the dynamical contribution to the transfer of spectral weight in the optical data on LSNO as can be seen in the data by Ido *et al.*[20] Up to now, it is not clear to us how to think about this length scale, and further theoretical work is needed to clarify the role of polaron physics with regard to transfer of spectral weight effects in the optical conductivity.[19] On the other hand, the similarity between the cuprate NEXAFS and optical data points out that in this metallic compound quantum effects also play a role on large length scales, as can be seen from their occurrence in the optical data.

In summary, although it is hard to quantify the data, we conclude that the holes are still quantum mechanical on the scale of a lattice constant and the system is *not in the small polaron regime* as defined by Eq. (5.12). This is not entirely surprising. The only reason to believe in small polarons comes from semiclassical calculations which are known to yield a lower bound only for the polaron coherence length.[6,7] At the same time, our finding gives some insight into the nature of the ordering phenomena occurring in the doped nickelates. *Quantum mechanics plays a role in the formation of polaron lattice*[9] *and domain wall*[10] *phases found in the doped nickelate*. As usual, one has to compare the quantum coherence length of the particles, ξ, with the interparticle distance as implied by the ordering, l. If $\xi \ll l$ one is dealing with a fully classical crystal, while the opposite limit is of relevance, e.g., to BCS superconductors. Consider the polaron lattice, discovered by Chen *et al.*[9] for $x=0.5$. If the polarons were classical, they would occupy every other lattice site so that $l = 2a_0 > \xi$, where a_0 is the lattice constant. From the NEXAFS data we infer that $\xi > 2a_0$ and it follows that the polarons have substantial overlaps. This is consistent with other observations. For instance, at $x=0.33$ a rather dense striped phase of charged domain walls is believed to exist.[9] Although at least perpendicular to the walls $l > 2a_0$, Chen *et al.* do not find higher harmonics, implying that the width of the domain walls (due to quantum zero-point motion, i.e., ξ) is at least of order of their mutual separation. Finally, even at $x \approx 0.20$ where the third harmonic has been found,[10] the latter is quite weak indicating that the width of the walls is still of order of the wall-wall distance $\sim 4a_0$.

VI. SUMMARY

We have performed polarization-dependent x-ray absorption measurements near the O 1*s* and Ni 2*p* edges of $La_{2-x}Sr_xNiO_{4+\delta}$ single crystals over a wide doping range of $0 \leqslant x \leqslant 0.6$. From a comparison with the same kind of data on $La_2CuO_{4+\delta}$ and NiO, we get direct evidence for the differences in the energetic ordering of states with different atomic character and orbital symmetry close to the Fermi level between the undoped compounds. The underlying reason for this is the different size of the Jahn-Teller distortion within the $Ni(Cu)O_6$ octahedra, resulting in a tetragonal crystal-field splitting E_z of about 1.3 eV between the e_g orbitals (x^2-y^2 and $3z^2-r^2$) of the transition metal atom in $La_2NiO_{4+\delta}$ as well as the difference in the *d*-band filling.

From a detailed comparison of the experimental spectra of doped LSNO with results from cluster calculations using an appropriate parameter set based on that of NiO, we find that the prepeaks in the polarization-dependent O 1*s* NEXAFS spectra can be assigned to the low-lying $^3B_1$ final state, including *d*-*d* excitons leading to $^1A_1$ and $^1B_1$ sidebands for $\mathbf{E} \| \mathbf{c}$ and $\mathbf{E} \| \mathbf{a}$, respectively. The results yield an energy difference between the high- and low-spin states of the undoped $La_2NiO_{4+\delta}$ of ~ 0.3–0.6 eV corresponding to the $^3B_1$-$^1A_1$ separation. Furthermore, the observation of the $^3B_1/^1B_1$ doublet gives direct evidence for the Zhang-Rice nature of the doped carriers in LSNO.

Since the Sr dependence of the intensity of the doping-induced prepeaks in LSNO exhibits a distinct dynamical contribution to the transfer of spectral weight, we conclude that the polarons in doped LSNO can be considered as quantum-mechanical objects on a length scale of the order of a lattice constant. Thus the polarons seem to have a substantial overlap and therefore LSNO cannot be considered as being in the small polaron regime. Together with the structural information from other experiments, this raises the question whether the observed formation of polaron domain walls and polaron lattices has to be considered as a result of this large quantum coherence length.

ACKNOWLEDGMENTS

J.Z. acknowledges financial support by the Dutch Royal Academy of Sciences (KNAW) and E.P. by the HSP II/AUFE program of the German Academic Exchange Service (DAAD). The experimental part of this work was done at the National Synchrotron Light Source, which is supported by the U.S. Department of Energy under Contract No. DE-AC02-76CH00016.

*Present address: Materials Science Centre, University of Groningen, NL-9747 AG Groningen, The Netherlands.
†Present address: Synchrotron Radiation Research Center, Hsinchu Science-Based Industrial Park, Hsinchu, Taiwan.

[1] R. J. Cava, B. Batlogg, T. T. Palstra, J. J. Krajewski, W. F. Peck, Jr., A. P. Ramirez, and L. W. Rupp, Jr., Phys. Rev. B **43**, 1229 (1991).
[2] Y. Takeda, R. Kanno, M. Sakano, O. Yamamoto, M. Takano, Y. Bando, H. Akinaga, K. Takita, and J. B. Goodenough, Mater. Res. Bull. **25**, 293 (1990).
[3] Z. Kakol, J. Spałek, and J. M. Honig, J. Solid State Chem. **79**, 288 (1989).
[4] Th. Strangfeld, K. Westerholt, and H. Bach, Physica C **183**, 1 (1991).
[5] X.-X. Bi and P. C. Eklund, Phys. Rev. Lett. **70**, 2625 (1993); X.-X. Bi, P. C. Eklund, and J. M. Honig, Phys. Rev. B **48**, 3470 (1993).
[6] V. I. Anisimov, M. A. Korotin, J. Zaanen, and O. K. Andersen, Phys. Rev. Lett. **68**, 345 (1992).
[7] J. Zaanen and P. B. Littlewood, Phys. Rev B **50**, 7222 (1994).
[8] F. C. Zhang and T. M. Rice, Phys. Rev. B **37**, 3759 (1988).
[9] C. H. Chen, S.-W. Cheong and A. S. Cooper, Phys. Rev. Lett. **71**, 2461 (1993).
[10] J. M. Tranquada, D. J. Buttrey, V. Sachan, and J. E. Lorenzo, Phys. Rev. Lett. **73**, 1003 (1994); also S. M. Hayden, G. H. Lander, J. Zarestky, P. J. Brown, C. Stassis, P. Metcalf, and J. M. Honig, *ibid.* **68**, 1061 (1992).
[11] J. van Elp, H. Eskes, P. Kuiper, and G. A. Sawatzky, Phys. Rev. B **45**, 1612 (1992).
[12] H. Romberg, M. Alexander, N. Nücker, P. Adelmann, and J. Fink, Phys. Rev. B **42**, 8768 (1990).
[13] E. Pellegrin, N. Nücker, J. Fink, S. L. Molodtsov, A. Guttierez, E. Navas, O. Strebel, Z. Hu, M. Domke, G. Kaindl, S. Uchida, Y. Nakamura, J. Markl, M. Klauda, G. Saemann-Ischenko, J. L. Peng, Z. Y. Li, and R. L. Greene, Phys. Rev. B **47**, 3354 (1993).
[14] C. T. Chen, L. H. Tjeng, J. Kwo, H. L. Kao, P. Rudolf, F. Sette, and R. M. Fleming, Phys. Rev. Lett. **68**, 2543 (1992).
[15] H. Eskes and G. A. Sawatzky, Phys. Rev. B **43**, 119 (1991); H. Eskes, M. B. J. Meinders, and G. A. Sawatzky, Phys. Rev. Lett. **67**, 1035 (1991); M. B. J. Meinders, H. Eskes, and G. A. Sawatzky, Phys. Rev. B **48**, 3916 (1993).
[16] A. B. Harris and R. V. Lange, Phys. Rev. **157**, 295 (1967).
[17] M. S. Hybertsen, E. B. Stechel, W. M. C. Foulkes, and M. Schlüter, Phys. Rev. B **45**, 10 032 (1992).
[18] L. F. Feiner, Phys. Rev. B **48**, 16 857 (1993).
[19] H. Eskes and A. M. Oleś, Phys. Rev. Lett. **73**, 1279 (1994).
[20] T. Ido, K. Magoshi, H. Eisaki, and S. Uchida, Phys. Rev. B **44**, 12 094 (1991).
[21] Taihei Nitadori, Motohiko Muramatsu, and Makoto Misono, Bull. Chem. Soc. Jpn. **61**, 3831 (1988).
[22] W. J. Veigele, in *Handbook of Spectroscopy*, edited by J. W. Robinson (CRC, Cleveland, OH, 1974), Vol. 1, pp. 28–154.
[23] D. D. Vvedensky, in *Unoccupied Electronic States*, edited by J. E. Fuggle and J. E. Inglesfield (Springer-Verlag, Berlin, 1992).
[24] L. F. Mattheiss, Phys. Rev. Lett. **58**, 1028 (1987).
[25] G. Y. Guo and W. M. Temmerman, Phys. Rev. B **40**, 285 (1989).
[26] W. M. Temmerman, Z. Szotek, and H. Winter, Phys. Rev. B **47**, 11 533 (1993).
[27] A. Svane, Phys. Rev. Lett. **68**, 1900 (1992).
[28] M. T. Czyzyk and G. A. Sawatzky, Phys. Rev. B **49**, 14 211 (1994); and unpublished results.
[29] P. Kuiper, J. van Elp, G. A. Sawatzky, A. Fujimori, S. Hosoya, and D. M. Leeuw, Phys. Rev. B **44**, 4570 (1991).
[30] P. Kuiper, G. Kruizinga, J. Ghijsen, G. A. Sawatzky, and H. Verweij, Phys. Rev. Lett. **62**, 221 (1989).
[31] P. Kuiper, D. E. Rice, D. J. Buttrey, L. H. Tjeng, and C. T. Chen, Physica B **208&209**, 271 (1995).
[32] J. Zaanen and A. M. Oleś, Phys. Rev. B **48**, 7197 (1993).
[33] J. B. Grant and A. K. McMahan, Physica C **162–164**, 1439 (1989).
[34] R. Newman and R. M. Chrenko, Phys. Rev. **114**, 1507 (1959).
[35] S. Uchida, T. Ido, H. Takagi, T. Arima, Y. Tokura, and S. Tajima, Phys. Rev. B **43**, 7942 (1991); S. Tajima, H. Ishii, T. Nakahashi, S. Uchida, M. Seki, S. Suga, Y. Hidaka, M. Suzuki, T. Murakami, K. Oka, and H. Unoki, J. Opt. Soc. Am. B **6**, 475 (1989).
[36] G. van der Laan, C. Westra, C. Haas, and G. A. Sawatzky, Phys. Rev. B **23**, 4369 (1981).
[37] A. Fujimori, F. Minami, and S. Sugano, Phys. Rev. B **29**, 5225 (1984).
[38] J. Zaanen, in *Unoccupied Electronic States* (Ref. 23); H. Eskes, L. H. Tjeng, and G. A. Sawatzky, Phys. Rev. B **41**, 288 (1990).
[39] J. Zaanen, G. A. Sawatzky, and J. W. Allen, Phys. Rev. Lett. **55**, 418 (1985); J. Zaanen and G. A. Sawatzky, J. Solid State Chem. **88**, 8 (1990).
[40] W. A. Harrison, *Electronic Structures and the Properties of Solids* (Freeman, San Francisco, 1980).
[41] A. K. McMahan, R. M. Martin, and S. Sathpathy, Phys. Rev. B **38**, 6650 (1988).
[42] T. A. Kaplan, H. Chang, S. D. Mahanti, and J. F. Harrison, in *Fundamental Materials Science*, edited by M. F. Thorpe (Plenum Press, New York, 1994), Vol. 1.
[43] A. M. Oleś, L. F. Feiner, and J. Zaanen, J. Magn. Magn. Mater. (to be published).
[44] S. Sugai *et al.*, Phys. Rev. B **42**, 1045 (1990).
[45] C. T. Chen, F. Sette, Y. Ma, M. S. Hybertsen, E. B. Stechel, W. M. C. Foulkes, M. Schluter, S.-W. Cheong, A. S. Cooper, L. W. Rupp, Jr., B. Batlogg, Y. L. Soo, Z. H. Ming, A. Krol, and Y. H. Kao, Phys. Rev. Lett. **66**, 104 (1991).
[46] G. A. Sawatzky (unpublished).
[47] G. D. Mahan, *Many Particle Physics* (Plenum Press, New York, 1981).
[48] J. Zaanen (unpublished).